Available online at www.sciencedirect.com
ScienceDirect
Cement & Concrete Composites 29 (2007) 533–541
Cement & Concrete Composites
www.elsevier.com/locate/cemconcomp

# Microstructure and performance of energetically modified cement (EMC) with high filler content

H. Justnes [a,*], P.A. Dahl [a], V. Ronin [b], J.-E. Jonasson [b], L. Elfgren [b]

[a] SINTEF Concrete, Trondheim, Norway
[b] Division of Structural Engineering, Luleå University of Technology, Sweden

Received 4 January 2006; received in revised form 29 January 2007; accepted 14 March 2007
Available online 24 March 2007

**Abstract**

Energetically modified cement (EMC) has been produced by high intensive grinding/activation of normal portland cement (NPC) together with 20% and 50% quartz sand. EMC concretes were compared to NPC based concrete using the *k*-factor concept. The *k*-factor for concrete with w/c = 0.60–0.45 was 0.7–0.9 for 1 d and 1.1–1.3 for 28 d compressive strength. $k > 1$ for both capillary suction, porosity, vapor diffusion and chloride permeability. For carbonation resistance *k* was ≈0.55.

Microstructure of EMC paste with 50% quartz sand and w/c = 0.40 showed that the quartz was extensively ground and formed agglomerates with cement having a high inner surface. The degree of hydration of the cement in EMC was as high as 71% after 1 d compared to 45% for untreated blend. Refined pore size distribution of EMC versus the blend means that even for equal hydration at higher ages EMC will perform better.


*Keywords:* Blended cement; Environment; Filler; Microstructure; Performance

## 1. Introduction

From the beginning of 1990s extensive study of the energetically modified cement (EMC) produced by high intensive grinding/activation of normal portland cement (NPC) together with different types of fillers has been performed by Luleå University of Technology, EMC Development AB, Sweden, and SINTEF, Norway, as published by Ronin et al. [1–4], Jonasson et al. [5] Rao et al. [6], Groth et al. [7], Hedlund et al. [8], Johansson et al. [9], Sellevold [10] and Ronin [11]. The EMC technology with 50% filler replacing NPC may have substantial impact on the environment since it enables an approximately 40% cut in $CO_2$ outlet.

This paper presents properties and performance of concrete based on EMC containing 20% and 50% quartz filler (weight percentage) as compared to concrete based on NPC. Furthermore, the microstructure of EMC paste versus paste from a simple blend of NPC and 50% quartz was compared to explain the mechanism of the improved performance. The microstructure part is presented in more detail by Justnes et al. [12] together with EMC based on fly ash instead of quartz sand.

## 2. Experimental

### 2.1. Materials

Normal portland cement (NPC) denoted CEM I, 42.5 according to EN 197-1 and type I according to ASTM C150 was used. The cement was manufactured by Cementa AB, Sweden and had the following composition: 65.7% CaO, 19.7% $SiO_2$, 5.5% $Al_2O_3$, 2.8% $Fe_2O_3$, 2.6% $SO_3$, 0.1% $Na_2O$ and 1.6% $K_2O$.

Quartz filler obtained by preliminary grinding of quartz sand to 100% passing 250 μm was used. The composition

* Corresponding author.
*E-mail address:* harald.justnes@sintef.no (H. Justnes).

0958-9465/$ - see front matter © 2007 Elsevier Ltd. All rights reserved.
doi:10.1016/j.cemconcomp.2007.03.004

of quartz was 2.2% CaO, 73.9% $SiO_2$, 13.1% $Al_2O_3$, 2.6% $Fe_2O_3$, <0.02% $SO_3$, 3.4% $Na_2O$ and 3.9% $K_2O$.

EMCs with 20% (EMC20) and 50% (EMC50) quartz replacing NPC by weight, respectively, were produced by intergrinding NPC and quartz filler in a Humboldt Palla 20U vibrating mill. The blends of 2 kg material were subjected to milling for 30 min with porcelain cylindrical grinding media with 10 mm diameter and 150 rpm vibrating cycle. The EMC cements had fineness 471 $m^2/g$ (Blaine) and EN mortar compressive strengths of >26 MPa and >42.5 MPa after 2 and 28 d of curing, respectively.

The natural sand and crushed gravel for the concrete were produced by NorStone AS in Årdal, Norway.

For the mechanism study, the 50/50 quartz/cement prepared by the EMC technology was denoted EQ, while a simple 50/50 blend of the powders was denoted Q. Pastes were made of EQ and Q with w/c = 0.40 using distilled water, filled on glass vials and rotated perpendicular to their axes until set to avoid separation. Hydration was stopped at different termini by crushing, replacing free water by ethanol and drying at 105 °C. Calculated initial volume fractions of these pastes were 53 vol% water, 21 vol% cement and 26 vol% quartz.

### 2.2. Methods

The three concrete mixes produced with each binder (NPC, EMC-20 and EMC-50) were made with water/binder-ratios (w/b) of 0.45, 0.50 and 0.60, and designed to have the same binder content in $kg/m^3$ for each w/b. The concrete compositions are given in Table 1. All concrete mixtures were blended in an Eirich 50 l forced action mixer, using the procedure described EN 480-1.

Measurements of slump, spread, apparent density and air content were performed according to ISO 4109, prEN 1015-13, ISO 6276 and ISO 4848, respectively. Furthermore, the temperature development in 15 l of concrete placed in a 100-mm thick box of expanded polyurethane was measured continuously during more than 72 h. From this, the adiabatic temperature and heat development, as well as the isothermal heat release were calculated. The setting time was determined as the time for accumulated heat to exceed 12 kJ/kg binder more than the base line (see Tables 2 and 3 for results).

Compressive strength was determined after 1, 2, 7, 28 and 90 d as a mean of 2 (7 d), 3 (1, 2 and 90 d) and 4 (28 d) specimens for each mix. 100 mm cubes were used as test specimens. Molding, curing conditions and test procedure were in accordance with ISO 4012.

Apparent chloride diffusion coefficients (i.e. migration coefficients) according to Fick's 1st law of diffusion, and time for chlorides to penetrate the specimen, were measured on concrete discs of dimension 100 mm diameter × 50 mm thickness sawn from a 91 d old cylinder of dimension 100 mm diameter × 200 mm length cured at 20 °C in water. The specimen is placed between two compartments filled with 3% NaCl solution (compartment 1 with chloride concentration $C_1$) and 0.3 N NaOH solution (compartment 2), respectively. In both solution a metal screen is place close to the concrete surface and a constant direct current potential of $\Delta U = 12$ V is applied between them (Fig. 1). The electric resistivity of the specimen is monitored before and after the experiment. Due to the electric field, the chloride ions will migrate through the concrete from the NaCl compartment to the NaOH compartment. The concentration of chloride ion ($C_2$) in the NaOH compartment as a function of time ($t$) is determined and the results plotted like the sketch in Fig. 2.

When a straight line is obtained between the five last data points, $\Delta C_2/\Delta t$ is determined as the slope of this line as shown in Fig. 2. Assuming that migration is the dominating transport mechanism and that diffusion and convec-

Table 1
Concrete composition

| Binder type | Material composition, $kg/m^3$ | | | | w/b-ratio[c] |
|---|---|---|---|---|---|
| | Binder | Water[a] | Aggregate[b] | Mighty 150 | |
| NPC | 367 | 163 | 1886 | 3.4 | 0.45 |
| | 331 | 164 | 1912 | 2.8 | 0.50 |
| | 274 | 164 | 1960 | 2.2 | 0.60 |
| EMC-50 | 361 | 160 | 1854 | 4.5 | 0.45 |
| | 328 | 163 | 1895 | 3.8 | 0.50 |
| | 274 | 164 | 1960 | 3.0 | 0.60 |

[a] Neither water absorbed in aggregates nor water in Mighty 150 is included.
[b] Absorbed water is included.
[c] Water absorbed in aggregates is excluded, while water in Mighty 150 is included.

Table 2
Properties of fresh concrete

| Binder type | w/b-ratio | Concrete temp., °C | Consistency, mm | | App. density, $kg/m^3$ | Air vol.% |
|---|---|---|---|---|---|---|
| | | | Slump | Spread | | |
| NPC | 0.45 | 21 | 110 | 420 | 2420 | 2.0 |
| | 0.50 | 21 | 90 | 390 | 2410 | 2.2 |
| | 0.60 | 21 | 105 | 425 | 2400 | 2.1 |
| EMC-50 | 0.45 | 21 | 85 | 395 | 2380 | 2.1 |
| | 0.50 | 21 | 90 | 390 | 2390 | 1.9 |
| | 0.60 | 21 | 80 | 370 | 2400 | 1.5 |

Table 3
Setting time and heat of hydration for concrete

| Binder type | w/b-ratio | Time of setting, h–min | | Isothermal heat, kJ/kg binder | Adiabatic $T$ increase, °C |
|---|---|---|---|---|---|
| | | Measured | Equivalent at 20 °C | | |
| NPC | 0.45 | 4–20 | 4–50 | 328 | 49 |
| | 0.50 | 4–00 | 4–30 | 342 | 45 |
| | 0.60 | 4–00 | 4–30 | 361 | 39 |
| EMC-50 | 0.45 | 3–50 | 4–40 | 316 | 47 |
| | 0.50 | 4–40 | 5–00 | 277 | 35 |
| | 0.60 | 4–50 | 5–10 | 281 | 29 |
| | 0.60 | 3–40 | 4–10 | 369 | 40 |

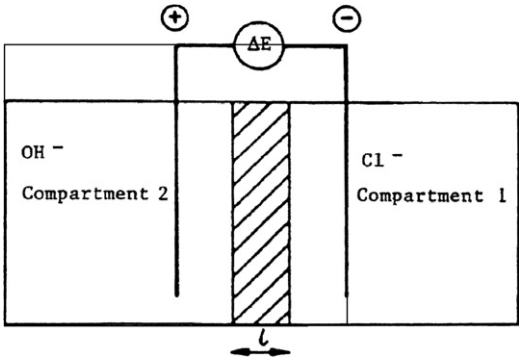


Fig. 1. Principle set-up of a chloride migration experiment.

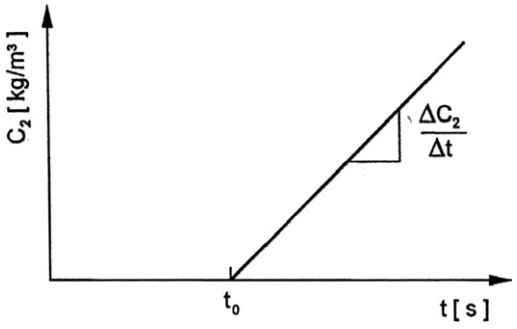


Fig. 2. Sketch of the chloride concentration in compartment 2 as a function of time.

tion can be neglected, the migration coefficient for chlorides can be determined by the formula

$$D_{\mathrm{m}} = \frac{R \cdot T \cdot \ell \cdot V_2}{z_{\mathrm{Cl}} \cdot F \cdot \Delta E \cdot \gamma_{\mathrm{Cl}} \cdot C_1 \cdot A} \cdot \frac{\Delta C_2}{\Delta t} \quad (1)$$

where $R$ = the universal gas constant = 8.314 J/mol K; $T$ = absolute temperature (K); $\ell$ = thickness of the sample (m); $V_2$ = volume of compartment 2 ($m^3$); $z_{Cl}$ = electrical charge of chloride = −1; $F$ = Faradays number = 96,500 C/equivalent; $\Delta E$ = voltage drop over the specimen (V); $\gamma_{Cl}$ = activity coefficient of chloride (taken as 1 here for simplicity); $C_1$ = chloride concentration in compartment 1 (kg/$m^3$) or (mol/l); $A$ = cross-sectional area of sample ($m^2$); $\Delta C_2/\Delta t$ = steady state change in chloride concentration versus time in compartment 2 (kg/$m^3$ s) or (mol/l s).

It should be noted that the voltage drop across the specimen, $\Delta E$, is less than the applied voltage, $\Delta U$, given by

$$\Delta U = \Delta E + E^{\mathrm{rev}}_{\mathrm{H_2O}} + \eta \quad (2)$$

where $E^{\mathrm{rev}}_{\mathrm{H_2O}}$ = reversible dissociation potential of water = 0.463 V at 25 °C and pH 13 and $\eta$ = polarisation effects (V). In this study $\Delta U = \Delta E$ for simplicity. The method is in accordance with NTBuild 355 [13].

The chloride concentration profiles of were measured on concrete discs of dimension 100 mm diameter × 50 mm thickness sawn from a cylinder of dimension 100 mm diameter × 350 mm length stored at 20 °C in water for 90 d. Chloride diffusion coefficients, $D$, and chloride concentrations at the surface, $C_0$, can then be calculated with basis in Fick's 2nd law for non-steady state diffusion:

$$\frac{\mathrm{d}C}{\mathrm{d}t} = D\frac{\mathrm{d}^2C}{\mathrm{d}x^2} \quad (3)$$

The solution of Fick's 2nd law of diffusion (Eq. (3)) gives the chloride content as a function of exposure time, $t$, and distance from exposure surface, $x$:

$$C(x,t) = C_0 - (C_0 - C_i) \cdot \mathrm{erf}(x/\sqrt{4 \cdot D \cdot t}) \quad (4)$$

where $D$ = chloride diffusion coefficient; $C(x,t)$ = chloride concentration at depth $x$ at time $t$; $C_0$ = calculated surface concentration of chlorides; $C_i$ = original chloride content in the sample (background level); $x$ = depth from exposure surface; $t$ = exposure time; erf = error function (Eq. (5)).

$$\mathrm{erf}(z) = (2/\sqrt{\pi}) \cdot \int_o^z \exp(-u^2)\,\mathrm{d}u \quad (5)$$

The chloride diffusion coefficient, $D$, and chloride concentration at the surface, $C_0$, are calculated by fitting Eq. (4) to the measured chloride profile by non-linear regression analysis. The outer layer (0–1 mm) is omitted from the regression analysis. The method is described in detail in NTBuild 443 [14].

Chloride penetration (i.e. migration in 60 V electrical field) was measured on concrete discs of dimension 100 mm diameter × 50 mm thickness sawn from a cylinder of dimension 100 mm diameter × 200 mm length cured at 20 °C in water for 90 d. Recording of current flow, calculation of charge passed and evaluation of the results followed the criteria given in ASTM C1202-94.

The reason for employing all three of the preceding "chloride ingress" tests is that all of them are much used in literature. However, the non-steady diffusion test is believed to be more in line with concrete submersed in sea water in the field (and even in the tidal zone), while the to others gives results that are more or less proportional with conductivity relevant for propagating corrosion of rebars initiated by chlorides.

Water vapor diffusion coefficients (Fick's 1st law) were measured on sawn concrete discs of 100 mm diameter × 20 mm thickness at an age of 28 d according to NTBuild 369 [15] with a difference in humidity over the specimen from 100% to 50% RH.

A concrete cylinder (150 mm diameter × 300 mm thickness) was used for the production of three specimens of dimension 150 mm diameter × 90 mm thickness by sawing at 1 d age. Specimens were stored at 20 °C in humid air (≈100% RH) for 27 d (total age 28 d). Water penetration was tested by applying water pressures of 0.3, 0.5 and 0.7 MPa (24 h at each pressure) to one end surface of each specimen with penetration zone 75 mm in diameter and 90 mm in height. Water penetration depths were measured immediately after splitting at the end of the testing period by visual inspection (dark grey = wet zone).

The capillary suction tests and calculations were performed as described in detail by Justnes et al. [16], but the

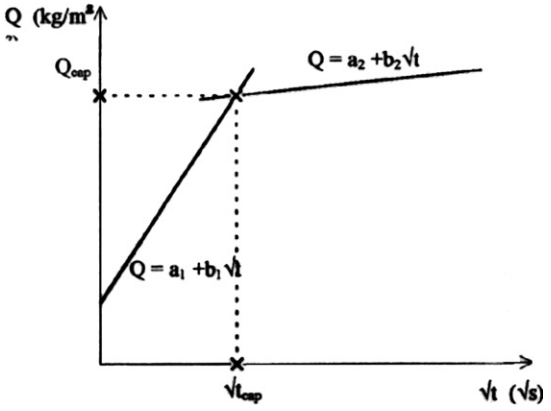


Fig. 3. Principle of water absorption by a sample in the capillary suction test.

utilized formulas are repeated here. The specimens were discs with diameter 100 mm and thickness 20 mm, cut from 200 mm high cast cylinders. Each mix was represented by four parallel specimens, tested after 90 d water curing. After drying at 105 °C the discs are placed on a grating 1 mm below the water surface in a covered box. The increase in weight as the specimen suck water is monitored for 5 d and plotted versus square root of time as sketched in Fig. 3.

The results from the capillary suction test can be expressed by means of linear regression analysis. Two lines are obtained; the first line represents the values until the water front reaches the top of the specimen and the second line the values thereafter. The crossing between the two straight lines is calculated and expressed by the water absorption value ($Q_{cap}$) and time for exposure ($t_{cap}$). These values can be used to calculate the capillary coefficient, $k$, and the resistance coefficient, $m$;

$$k = \frac{Q_{cap}}{\sqrt{t_{cap}}} \quad (kg/m^2\sqrt{s}) \tag{6}$$

$$m = \frac{t_{cap}}{h^2} \quad (s/m^2) \tag{7}$$

where $h$ is the thickness of the concrete sample. Thus, the capillary coefficient, $k$, gives an estimate of the velocity by which the concrete absorbs water, while the resistance coefficient, $m$, indicates the time needed for the water front to reach the top.

The procedure consist of six important steps for the specimen:

1. Drying to constant weight ($W_1$).
2. Capillary suction for 5 d with weight monitoring.
3. Water saturation by submersion 3 d in water at 1 atm ($W_2$).
4. Pressure saturation by submersion 3 d in water at 80 atm ($W_3$).
5. The outer volume ($V$) is recorded by differential weighing the specimen under water and saturated surface dry in air according to the principle of Archimedes.
6. Drying the specimen to constant weight at 105 °C ($W_4$).

From these six steps, one can calculate the initial moisture content, total porosity ($\varepsilon_{tot}$), the capillary porosity ($\varepsilon_{cap}$), the air volume ($\varepsilon_{air}$), the average density of the concrete solids ($\rho_{sol}$) and the dry density of the concrete ($\rho_{dry}$) according to the following formulas:

$$\text{Initial moisture} = \frac{(W_1 - W_4)\times 100\%}{V\cdot\rho_w} \ (\text{vol.}\%) \tag{8}$$

$$\varepsilon_{tot} = \frac{(W_3 - W_1)\times 100\%}{V\cdot\rho_w} \ (\text{vol.}\%) \tag{9}$$

$$\varepsilon_{cap} = \frac{(W_2 - W_1)\times 100\%}{V\cdot\rho_w} \ (\text{vol.}\%) \tag{10}$$

$$\varepsilon_{air} = \frac{(W_3 - W_2)\times 100\%}{V\cdot\rho_w} \ (\text{vol.}\%) \tag{11}$$

$$\rho_{sol} = \frac{W_1}{V - \frac{(W_3 - W_1)}{\rho_w}} = \frac{W_1}{V\cdot(1 - \varepsilon_{tot}/100\%)} \ (kg/m^3) \tag{12}$$

$$\rho_{dry} = \frac{W_1}{V} \ (kg/m^3) \tag{13}$$

The carbonation resistance was measured on concrete prisms (70 mm height, 70 mm width and 300 mm length) water cured for 28 d followed by drying at 45 °C in a ventilated oven for 7 d prior to storage for 16 weeks in 3% $CO_2$ in a carbonation chamber at 23 °C and 60 ± 10% RH. After 2, 4, 8, 12 and 16 weeks in $CO_2$ chamber, a ≈50 mm long slice was split off each specimen. Phenolphthalein was applied on the freshly broken surface of the slice and the carbonation depth measured from each of its four side surfaces. After the 16 weeks measurement of carbonation depths, the water content of the remaining part of each specimen was determined by weighing prior to, and after drying at 105 °C to constant weight.

The porosity and pore size distribution of EQ and Q pastes were characterized by mercury intrusion porosimetry (MIP) and helium pychnometry (HeP). Chemical bound water and amount of calcium hydroxide was determined by thermal analyses (DTA/TG). Differences in microstructure of the paste were studied by scanning electron microscopy (SEM).

## 3. Results and discussion

### 3.1. Fresh and young concrete properties and compressive strength evolution

The properties of the fresh and young hardening concrete are presented in Tables 2 and 3 and show that the influence of EMC-50 on the important fresh concrete properties workability, stability, air content and time of setting is not significantly different from the influence of the NPC cement used to produce EMC binder. However, the dosage of superplasticizer (Mighty 150, 40% solution) needed to produce the required consistency at each w/b-ratio was somewhat higher for the EMC mixes than for the NPC reference mixes (Table 1). The EMC-50 generated a total heat per unit weight equal to the heat of the reference NPC

cement liberation, which in combination with the strength development (Fig. 4) of EMC concrete, indicates significant chemical activation of the portland clinker and possibly quartz components in EMC.

The compressive strength development of NPC and EMC-50 concrete in Fig. 4 demonstrates slightly lower early age strengths (1 and 2 d curing time) for EMC and this difference is more pronounced with increased w/b. EMC reached compressive strength equal to NPC at about 7 d of hardening and exhibited strength superior to NPC concrete after 28 and 90 d reaching strength levels of ≈40 MPa and 70 MPa for w/b = 0.60 and 0.45, respectively. The *k*-value evaluated according to prEN206 for concrete with w/c = 0.60–0.45 was 0.7–0.9 for 1 d compressive strength and 1.1–1.3 for 28 d compressive strength.

Standard mortars (EN197) made from EQ cement exhibited 1, 3, 7 and 28 d compressive strengths of 10.4 ± 0.4, 18.3 ± 0.7, 21.8 ± 0.7 and 32.7 ± 1.2 MPa, respectively, while the analogue values for Q blend were 1.8 ± 0.2, 4.5 ± 0.3, 5.7 ± 0.3 and 8.4 ± 0.4 MPa. Early strength is generally much higher for EMC than for blends while they approach each other on longer term. The particular low strength of the Q blend versus EQ mortars is here due to the coarseness of the non-processed quartz and some separation.

### 3.2. Chloride ingress

Test results of the chloride ingress of EMC and NPC concrete; apparent diffusion coefficients, effective diffusion coefficients and resistance to chloride penetration are presented in Figs. 5a and b and Table 4, respectively.

The EMC concrete showed a considerably higher resistance to chloride penetration relative to the NPC concrete at similar w/b. Chloride diffusion coefficients of EMC concrete are significantly lower relative to NPC concrete, especially with increased w/b. For w/b = 0.60 the diffusion coefficients for EMC are only 50% of the coefficients for NPC concrete. Concrete produced with EMC containing 20% and 50% of quartz filler by NPC replacement showed comparable levels for diffusion coefficients.

The resistance to chloride penetration was also significantly higher for concrete made with EMC-50 than with NPC concrete. At 91 d age, the total charge passed has a

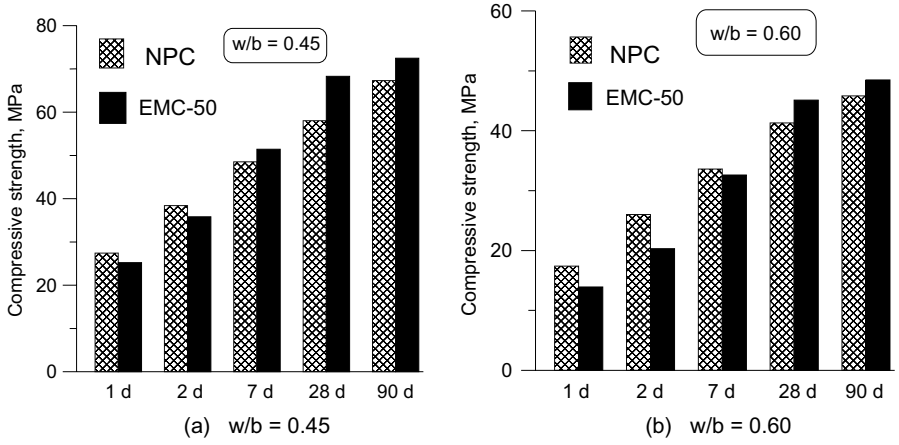


Fig. 4. Compressive strength tests (100 mm cube) according to ISO 4012.

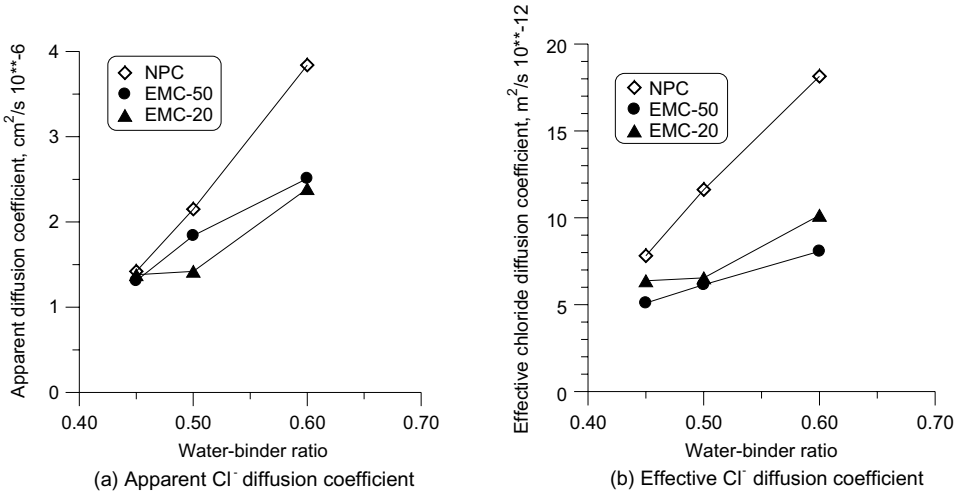


Fig. 5. Chloride ingress accelerated by electrical field under steady state conditions (a) and $Cl^-$ concentration under non-steady state conditions (b).

Table 4
Results from the testing of chloride permeability (ASTM C 1202-94)

| Binder type | w/b-ratio | Average "Charge passed" in Coulombs ± standard deviation | Evaluation of chloride permeability |
|---|---|---|---|
| NPC | 0.45 | 3734 ± 165 | Moderate |
| | 0.50 | 4030 ± 135 | High |
| | 0.60 | 4828 ± 448 | High |
| EMC-50 | 0.45 | 763 ± 62 | Very Low |
| | 0.50 | 821 ± 39 | Very Low |
| | 0.60 | 976 ± 106 | Very Low |
| EMC-20 | 0.45 | 1271 ± 141 | Low |
| | 0.50 | 1397 ± 55 | Low |
| | 0.60 | 1649 ± 185 | Low |

maximum of 4828 C for NPC with w/b = 0.60 and a minimum of 3734 C for NPC with w/b = 0.45, while for EMC-50 concrete analogue values were 976 and 763 C, respectively. Increasing the quartz filler content from 20% to 50% in EMC led to about 40% decrease of the average value of charge passed (w/b = 0.60).

### 3.3. Water transport

The data related to water transport evaluated by capillary suction, water vapor diffusion tests and water penetration are presented in Figs. 6, 7 and Table 5, correspondingly. Water transport estimates the potential ingress of water born aggressives in the concrete, which can cause deterioration of concrete and reinforcement. Also it is an indication of the potential degree of water saturation, which is directly correlated with the impact of freezing and thawing cycles on the concrete.

Rate of water transport by capillary suction was evaluated by the resistance number ($m$) according to Eq. (7), which is inversely related to the rate of water transport. EMC-50 concrete had much higher resistance number for the whole w/b range in comparison with NPC concrete. This could be attributed to increasing fineness of the pore system. Comparison of EMC-20 and EMC-50 concrete revealed that EMC-50 concrete had higher resistance numbers at lower w/b, but at w/b = 0.60 this parameter had about the same value for both concretes.

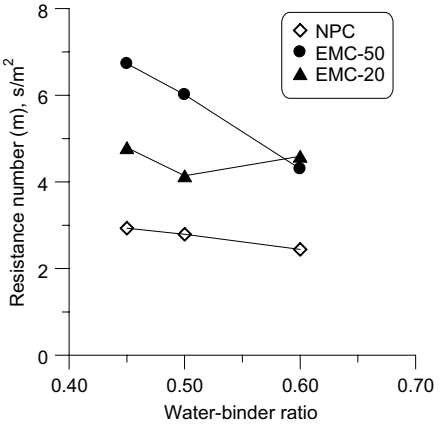


Fig. 6. Resistance number ($m$) from capillary suction testing.

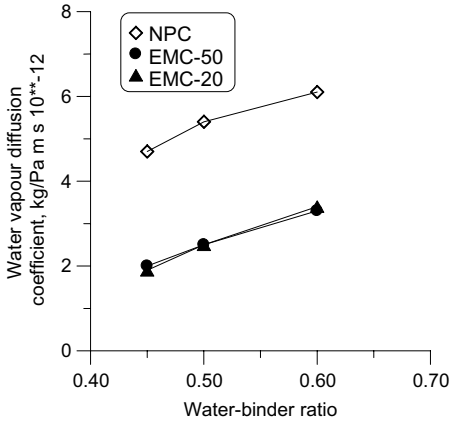


Fig. 7. Water vapor diffusion.

Table 5
Results from the measurements of the water penetration depths

| Binder type | w/b-ratio | Penetration depth, mm | | | |
|---|---|---|---|---|---|
| | | Average depth | | Maximum depth | |
| | | Individual | Mean | Individual | Mean |
| NPC | 0.45 | 5-5-10 | 7 | 15-10-25 | 17 |
| | 0.50 | 5-15-15 | 12 | 5-30-30 | 22 |
| | 0.60 | 5-5-5 | 5 | 25-10-15 | 17 |
| EMC-50 | 0.45 | 10-10-15 | 12 | 20-10-20 | 17 |
| | 0.50 | 5-5-5 | 5 | 15-15-10 | 13 |
| | 0.60 | 10-5-15 | 10 | 20-20-25 | 22 |

Similar tendencies could be observed for water vapor diffusion coefficients. Replacement of NPC by EMC-50 and EMC-20 led to considerable increase in resistance against water vapor diffusion. By comparing concrete at equal w/b, the water vapor diffusion through the EMC concrete was about 50% less than for the corresponding NPC concrete. In addition, the highest water vapor diffusion coefficient for the EMC mixes was substantially lower than the lowest for the NPC mixes, and there was no significant difference between EMC-50 and EMC-20 at a given w/b-ratio.

As can be seen from the mean values for average, as well as maximum, water penetration depths in Table 5, no significant influence of w/b or binder type could be observed. The test results show that all six investigated concrete compositions satisfy the requirements for resistance against water penetration given in the Norwegian code NS 3420 (individual average penetration depths <25 mm) and in prEN 206:1997 (maximum penetration <50 mm).

### 3.4. Carbonation resistance

Table 6 lists the test results with respect to resistance against carbonation. EMC-50 concrete had about twice

Table 6
Carbonation resistance for concrete

| Binder type | w/b-ratio | Average carbonation depth, mm | | | | |
|---|---|---|---|---|---|---|
| | | Storage time in 3% $CO_2$ and 60% RH, weeks | | | | |
| | | 2 | 4 | 8 | 12 | 16 |
| NPC | 0.45 | 5 | 6 | 7 | 6 | 7 |
| | 0.50 | 7 | 7 | 8 | 9 | 10 |
| | 0.60 | 4 | 5 | 9 | 12 | 13 |
| EMC-50 | 0.45 | 4 | 6 | 10 | 11 | 13 |
| | 0.60 | 7 | 11 | 16 | 19 | 21 |

the carbonation depth of NPC concrete. This is in line with existing knowledge regarding accelerated carbonation testing of concrete with blended cements. For pre-dried concrete, as in this test, the carbonation rate is mainly controlled by CaO, i.e. as CH and CSH, available for carbonation, which again depends on the amount of portland clinker.

In the EMC-50 case, the portland clinker content is reduced by 50%, but the expected reduced diffusion coefficient (in analogy to water vapor) may offset this effect. The accelerated drying employed (45 °C, 7 d) may accelerate carbonation further than by the increased $CO_2$ concentration (100× natural level) alone. This procedure may be unrealistic relative to actual conditions, and additional research is required to evaluate resistance against natural carbonation for EMC. This is supported by: (i) good historical field experience for other blended cements; (ii) improved resistance to water and chloride penetration for EMC; and (iii) finer and thus tighter pore structure of concrete based on EMC.

### 3.5. Pastes for mechanism studies

The solid particle densities of EQ and Q cements were measured by He-pycnometry to 2919 and 2900 kg/m$^3$, respectively. The specific surface, $S$ (m$^2$/kg), was measured for EQ to 566, 270, and 2210 by Blaine, particle size distribution (i.e. laser granulometry) and BET (i.e. $N_2$-adsorption), respectively. Analogue surfaces for Q were 260, 134 and 710 m$^2$/kg, respectively. The surface ratio BET/particle size = 8.2 and 5.3 for the powders EQ and Q, respectively, while the surface ratio BET/Blaine = 3.90 and 2.74 for the same powders. This indicates that the inner surface has increased more than the outer surface in the milling process, which can be subscribed to an increased number of cracks in individual particles or formation of agglomerates of finer particles. SEM of plane sections of powder cast in epoxy revealed that the milling process is highly efficient. It could be seen [12] that quartz and cement are ground and agglomerates of mixed fines of quartz and cement are formed, both on a larger scale as flakes (appearing as several 100 μm rods in the cross-section) and even as small grains of the size of normal cement grains.

Four features of the pastes were extracted from the DTA/TG curves at the different termini: Tot. = total mass loss from 105 °C to 1000 °C in percentage of the ignited powder = total chemical bound water. $\alpha$ = Degree of hydration for the 50% cement fraction assuming that 25% water is chemically bound in completely hydrated cement (about 23% according to Ref. [17]). CH = the content of calcium hydroxide in percentage of the ignited powder. CH/Tot = the ratio between calcium hydroxide and total chemical bound water content in percent. The results are given for EQ and Q pastes in Tables 7 and 8, respectively. The EQ paste reached 71% hydration already at 1 d, and was thereafter rather constant with only a marginal increase between 7 and 28 d to 76%. The hydration of the cement in Q is more gradual since it is much coarser, but the hydration of Q and EQ is equal at 28 d. The content of calcium hydroxide relative to the total chemical bound water increases for both EQ and Q until 3 d, and flattens then out on a rather equal level. The only exception is a marginal decrease for EQ at 28 d that could indicate a minor pozzolanic activity between CH and very small or strained quartz grains. The CH content in EQ and Q of about 11% corresponds to 22% in the cement paste, which is in line with the expected level (about 25% for fully hydrated cement). Samples were kept sealed for 1 year before they were added excess water and stored until 2.5 years age (950 d). The total mass losses after 950 d correspond to degree of hydration in excess of 100%, which probably is caused by some mass loss from the ground quartz sand (only 74% $SiO_2$) that would off-set all hydration degree. The degree of hydration at 950 d is however about equal for EQ and Q, but more striking is the reduced CH content for EQ indicating a pozzolanic reaction. Such a reaction could also contribute to a somewhat higher mass loss. The pH of the excess water was >13 at this time as measured by indicator paper.

The specific surface ($S_g$), particle density ($\rho_p$), solid density ($\rho_s$), mercury accessible porosity ($\varepsilon_{Hg}$) and helium

Table 7
Features from thermal analysis for EQ paste as a function of time

| Age | Tot. (%) | $\alpha$ (%) | CH (%) | CH/Tot. (%) |
|---|---|---|---|---|
| 6 h | 5.08 | 41 | 2.21 | 43 |
| 1 d | 8.88 | 71 | 8.10 | 91 |
| 3 d | 8.63 | 69 | 10.21 | 118 |
| 7 d | 8.89 | 71 | 10.31 | 116 |
| 28 d | 9.48 | 76 | 10.58 | 112 |
| 950 d | 14.5 | 116 | 12.13 | 84 |

Table 8
Features from thermal analysis for Q paste as a function of time

| Age | Tot. (%) | $\alpha$ (%) | CH (%) | CH/Tot. (%) |
|---|---|---|---|---|
| 12 h | 5.57 | 44 | 4.00 | 72 |
| 1 d | 5.63 | 45 | 4.81 | 85 |
| 3 d | 7.09 | 57 | 7.85 | 111 |
| 7 d | 8.37 | 67 | 9.67 | 115 |
| 28 d | 9.49 | 76 | 11.05 | 116 |
| 950 d | 14.2 | 114 | 14.63 | 103 |

Table 9
Specific surface ($S_g$), particle density ($\rho_p$), solid density ($\rho_s$), mercury accessible porosity ($\varepsilon_{Hg}$) and helium accessible porosity ($\varepsilon_{He}$) of EQ pastes as a function of curing time

| Age | $S_g$ ($m^2/g$) | $\rho_p$ ($kg/m^3$) | $\rho_s$ ($kg/m^3$) | $\varepsilon_{Hg}$ (vol%) | $\varepsilon_{He}$ (vol%) |
|---|---|---|---|---|---|
| 6 h | 11.58 | 1370 | 2720 | 45.8 | 49.6 |
| 1 d | 18.37 | 1475 | 2387 | 37.4 | 38.2 |
| 3 d | 20.57 | 1492 | 2323 | 34.5 | 35.8 |
| 7 d | 23.69 | 1456 | 2297 | 34.0 | 36.6 |
| 28 d | 24.13 | 1487 | 2268 | 33.5 | 34.4 |
| 950 d | 28.30 | 1500 | 2233 | 30.6 | 32.8 |

accessible porosity ($\varepsilon_{He}$) of the pastes as a function of curing time are given in Tables 9 and 10 for EQ and Q pastes, respectively. The pore size distributions for the pastes cured for 1, 28 and 950 d are plotted in Fig. 8. The general usual trends are that the porosity decreases as a function of time and the specific surface increases as a function of time as the pores becomes smaller in size but higher in numbers (e.g. gel pores). The He accessible porosity of the milled species is smaller than the blended analogues at any age until at least 7 d due to higher degree of hydration, but is rather equal at 28 d (as the chemical bound water and w/s are equal), but again somewhat smaller at 950 d indicating very dense hydration products. The average density of solids decreases as a function of time due to increasing amount of crystal water as hydration proceeds. The pore radii at half the porosity for pastes are extracted to be

Table 10
Specific surface ($S_g$), particle density ($\rho_p$), solid density ($\rho_s$), mercury accessible porosity ($\varepsilon_{Hg}$) and helium accessible porosity ($\varepsilon_{He}$) of Q pastes as a function of curing time

| Age | $S_g$ ($m^2/g$) | $\rho_p$ ($kg/m^3$) | $\rho_s$ ($kg/m^3$) | $\varepsilon_{Hg}$ (vol%) | $\varepsilon_{He}$ (vol%) |
|---|---|---|---|---|---|
| 12 h | 7.22 | 1441 | 2676 | 44.8 | 46.1 |
| 1 d | 8.91 | 1472 | 2599 | 40.4 | 43.4 |
| 3 d | 10.67 | 1450 | 2490 | 38.3 | 41.8 |
| 7 d | 13.14 | 1538 | 2431 | 35.1 | 36.7 |
| 28 d | 14.52 | 1571 | 2358 | 33.5 | 33.4 |
| 950 d | 17.63 | 1573 | 2391 | 30.0 | 34.2 |

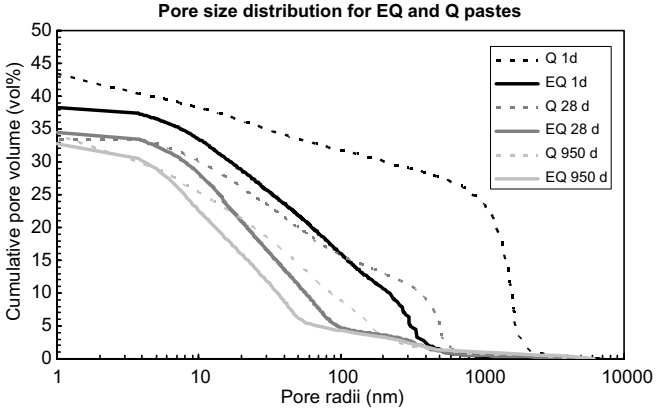


Fig. 8. Pore size distribution for EQ and Q paste (w/c = 0.40) after 1, 28 and 950 d curing.

435, 74, 45, 35, 30 and 22 nm at 6 h, 1 d, 3 d, 7 d, 28 d and 950 d for EQ paste, respectively, and 1,574, 1,254, 710, 298, 82 and 50 nm for Q paste after 12 h, 1 d, 3 d, 7 d, 28 d and 950 d curing.

Back scattered electron images (BEI) from SEM of cross-sections of paste from EQ and Q after 1 d curing are shown in Fig. 9. The general trends observed for the EQ and Q pastes by SEM are: (1) There are still agglomerates in the EQ paste that are not completely dispersed (no plasticizers was used), but to a much lesser extent than in the powder itself. (2) CH crystals prefer quartz as a substrate for growth. (3) There is little sign of pozzolanic reaction between calcium hydroxide and quartz within the 28 d of sealed curing. (4) Q paste has much coarser, regular CH crystals as compared to the more mass like CH morphol-

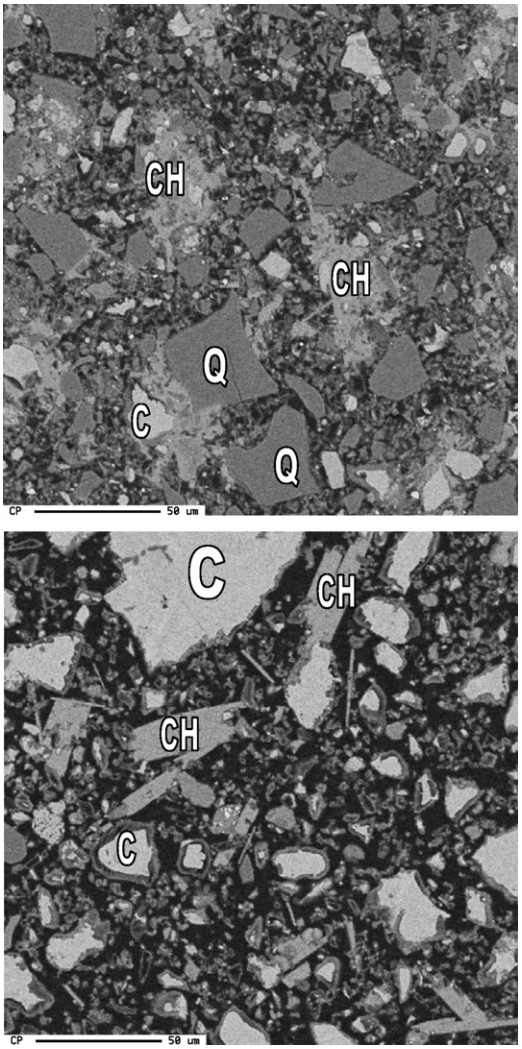


Fig. 9. BEIs (500×) of EQ (upper) and *Q* (lower) cured for 1 d. Calcium hydroxide regions are marked with CH in both cases. CH in EQ has an irregular, cloudy nature often embedding finer particles, while CH in Q appears as large platy crystals. Q binder appears much more porous (black area = pores) than EQ binder. This can explain difference in CH morphology, since CH crystals are given space to grow in the Q paste. Note also the more open reaction rims (CSH) around the cement grains in Q versus EQ. Cement and quartz grains are marked "C" and "Q".

ogy in EQ often embedding small quartz grains (example in Fig. 9). (5) Porosity is much higher in Q than in EQ pastes (see 1 d example in Fig. 9).

## 4. Conclusion

EMC concrete performed in line with concrete produced with normal portland cement (NPC) with respect to production properties (setting time, workability) and compressive strength.

Properties of importance for service life of concrete structures (e.g. vapor and water permeability, chloride ingress) are better for EMC than for NPC.

EMC performed not as well as NPC in the accelerated carbonation test, but in line with traditionally blended cements. Based on experience with other blended cements (e.g. high slag content), this is not expected to be a problem in practice. Significantly reduced vapor and water permeability in EMC concrete should contribute to increased carbonation resistance.

Microstructure investigations showed that improved performance of EMC (intensively milled 50/50 cement/quartz) versus NPC/filler blends can be explained by increased early hydration and better distribution of hydration products resulting in an extensive pore size refinement of the hardened binder. The pozzolanic activity of quartz filler determined after 950 d of curing also contribute positively to the long-term strength development and durability of EMC concrete.

## References

[1] Ronin V, Jonasson J-E. Investigation of the effective winter concreting with the usage of energetically modified cement (EMC) – material science aspects. Report 1994:03, Div. Structural Engineering Luleå University of Technology, Luleå, Sweden; 1994. 24 pp.

[2] Ronin V, Jonasson J-E. High strength and high performance concrete with use of EMC hardening at cold climate conditions. In: Proceedings of international conference on concrete under severe conditions, Sapporo, Japan, August 1995. p. 235–45.

[3] Ronin V, Jonasson J-E, Hedlund H. Advanced modification technologies of the Portland cement based binders for different high performance applications. In: Justnes H, editor. Proceedings of the 10th international congress on the chemistry of cement, Gothenburg, June 1997. Inform Trycket AB, Gothenburg, 2ii077, 8 pp (ISBN 91-630-5496-5).

[4] Ronin V et al. Method for producing cement, European Patent EP 0 696 261 B1; 1997. 13 pp.

[5] Jonasson J-E, Ronin V, Hedlund H. High strength concrete with energetically modified cement and modeling of shrinkage caused by self-desiccation. In: Proceedings of the 4th international symposium on the utilization of high strength/high performance concrete, Paris, France, August 1996. Paris: Presses Pont et Chausses; 1996. p. 245–54.

[6] Rao KH, Ronin V, Forssberg KSE. High performance energetically modified Portland blast-furnace cements. In: Justnes H, editor. Proceedings of the 10th International congress of the chemistry of cement. Gothenburg, June 1997. Inform Trycket AB, Gothenburg, 3ii104, 9 pp (ISBN 91-630-5497-5).

[7] Groth P, Ronin V. Influence of energetically modified cement on interfacial bond and fracture toughness in cement-based fiber reinforced composites. In: Holand I, Sellevold EJ, editors. Fifth international symposium on utilization of high strength/high performance cement, Sandefjord 20–24 June 1999. Oslo: Norwegian Concrete Association; 1999, ISBN 82-91341-25-7. p. 1114–23.

[8] Hedlund H, Ronin V, Jonasson J-E. Ecological effective high performance cement based binders. In: Holand I, Sellevold EJ, editors. Fifth international symposium on utilization of high strength/high performance cement, Sandefjord 20–24 June 1999. Oslo: Norwegian Concrete Association; 1999, ISBN 82-91341-25-7. p. 1144–53.

[9] Johansson K, Larsson C, Antzutkin ON, Forsling W, Rao KH, Ronin V. Kinetics of the hydration reactions in the cement paste with mechanochemically modified cement $^{29}$Si magic-angle-spinning NMR study. Cem Concr Res 1999;29:1575–81.

[10] Sellevold EJ. Summary and evaluation of SINTEF test results on energetically modified cements (EMC), SINTEF, Report Number STF22 F98764, 1998-09-18. 8 pp.

[11] Ronin V. A method of treating cement clinker. European Patent EP 0 975 557 B1; 2001. 6 pp.

[12] Justnes H, Elfgren L, Ronin V. Mechanism for performance of energetically modified cement versus corresponding blended cement. Cem Concr Res 2005;35:315–23.

[13] NTBuild 355: ''Concrete, mortar and cement based materials: chloride diffusion coefficients from migration cell experiments'', Edition 2, approved 1997-11, 4 pages (Can be obtained through www.nordtest.org).

[14] NTBuild 443: ''Concrete, hardened: accelerated chloride penetration'', Approved 1995-11, 5 pages (Can be obtained through www.nordtest.org).

[15] NTBuild 369: ''Concrete repair materials: water vapor diffusion'', Approved 1991-02, 3 pages (Can be obtained through www.nordtest.org).

[16] Justnes H, Thys A, Vanparijs F, Van Gemert D. Porosity and diffusivity of concrete with long-term compressive strength increase due to additions of the set accelerator calcium nitrate. In: Proceedings of the 9th international conference on durability of building materials and components, Brisbane, Queensland, Australia, 17th–20th March, 2002.

[17] Taylor HFW. Cement chemistry. 2nd ed. New York: Thomas Telford; 1997. p. 198.